

Article

The First Reaction Steps of Lithium-Mediated Ammonia Synthesis: Ab Initio Simulation

Dominykas Maniscalco¹, Dominik A. Rudolph¹ , Ebrahim Nadimi^{1,2}  and Irmgard Frank^{1,*} 

¹ Theoretical Chemistry, Leibniz University Hannover, Callinstr. 3A, 30167 Hannover, Germany; dominykas.maniscalco@stud.uni-hannover.de (D.M.); dominik.rudolph@stud.uni-hannover.de (D.A.R.); nadimi@kntu.ac.ir (E.N.)

² Faculty of Electrical Engineering, K. N. Toosi University of Technology, P.O. Box 16315-1355, Tehran 1996715433, Iran

* Correspondence: irmgard.frank@theochem.uni-hannover.de

Abstract: The reaction of molecular nitrogen with molecular hydrogen was simulated using ab initio molecular dynamics. The reaction was catalyzed by the addition of bulk lithium and oxygen. As is known from the experiment, the limiting step is the breaking of the nitrogen–nitrogen triple bond. We observed a mechanism that has not been discussed before: one of the nitrogen atoms of a nitrogen molecule is absorbed by the lithium bulk, whereas the other nitrogen atom reacts with hydrogen. Adding oxygen leads to a dominating reaction of oxygen with the lithium surface. The oxygen molecules break easily into single atoms and are, in part, absorbed by the lithium structure. Part of them remains on the surface and reacts with hydrogen. In this way, hydrogen is activated and can, in turn, react easily with molecular nitrogen. The overall reactivity as observed in the ab initio simulations reflects the extremely low density of lithium. Interstitial sites are readily occupied, leading to oxide and nitride structures.

Keywords: catalysis; reaction mechanisms; Car–Parrinello molecular dynamics



Citation: Maniscalco, D.; Rudolph, D.A.; Nadimi, E.; Frank, I. The First Reaction Steps of Lithium-Mediated Ammonia Synthesis: Ab-Initio Simulation. *Nitrogen* **2022**, *3*, 404–413. <https://doi.org/10.3390/nitrogen3030026>

Academic Editor: Stephen Macko

Received: 25 May 2022

Accepted: 27 June 2022

Published: 4 July 2022

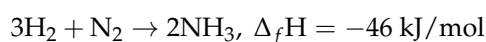
Publisher's Note: MDPI stays neutral with regard to jurisdictional claims in published maps and institutional affiliations.



Copyright: © 2022 by the authors. Licensee MDPI, Basel, Switzerland. This article is an open access article distributed under the terms and conditions of the Creative Commons Attribution (CC BY) license (<https://creativecommons.org/licenses/by/4.0/>).

1. Introduction

The formation of ammonia from the elements is a technologically important reaction [1,2].



The reaction is exothermic [3]. However, there is a huge barrier for the breaking of the N–N triple bond. In industry, the Haber–Bosch process is normally employed, which requires high pressures and high temperatures with iron as a catalyst. These extreme conditions result in a large CO₂ footprint. There is renewed interest in the ammonia formation as neither educt nor product contain or react to carbon dioxide [4–6]. This renewed interest is accompanied by more recent developments concerning reaction parameters and catalysts. For example, the lithium-mediated ammonia synthesis was investigated experimentally [7–9]. Remarkably, metallic lithium is able to split the nitrogen triple bond at ambient conditions [9]. The formation of Li₃N is considered to be the first reaction step. Surprisingly, an enhancement of the reaction by addition of oxygen was observed [10] which seems to be counter-intuitive: In the Haber–Bosch synthesis removal of oxygen is important. One would expect that oxygen poisons the lithium surface, reducing its ability to react with other species.

In the present study, we use Car–Parrinello molecular dynamics (CPMD), a method that belongs to the class of ab-initio molecular dynamics (AIMD) methods, to simulate the first reaction steps in this complex system. CPMD is a still-underestimated approach for the simulation of chemical reactions [11,12], in particular for surface reactions, see for example, refs. [13,14]. AIMD was applied before to the simulation of lithium ions in

electrochemical setups [15], but not in reactive simulations showing the lithium-mediated reaction mechanism of N_2 and H_2 .

CPMD solves the problem of how to describe nuclear motion in a very simple way, namely by using the classical approach as it is known from classical molecular dynamics (or force-field) calculations. The electronic structure is described quantum mechanically using density functional theory (DFT). The motion of the system is described semi-classically using the Car-Parrinello equations [11]. The electronic cloud follows the motion of the nuclei in every time step. With time steps of approximately 0.1 fs, it is possible to describe the dynamics of molecular systems on the scale of a few ps and of a few nm^3 . Chemical reactions are rare events and it is difficult to model them in a meaningful way. In particular, it is desirable to construct an equilibrated system with a well-defined temperature before observing reactions. Obtaining such equilibrated systems is often not easy or is even impossible. Equilibrated systems are characterized by a Maxwell–Boltzmann distribution of velocities that determines the temperature of the system. Fortunately, such a Maxwell–Boltzmann distribution develops quickly, typically within 0.1–0.2 ps, as it is the most likely distribution. Ideally, during this time, the system should be chemically stable. In contrast, during the production run, one would like to observe chemical reactions. The accuracy of the results and the computational cost are highly correlated to the density functional, which is used to approximate the quantum mechanical interaction between the electrons. A favourable cost–value ratio is obtained only for pure generalized gradient approximation (GGA) functionals, such as BLYP. The more accurate hybrid B3LYP method, using a mixture of BLYP exchange with Hartree-Fock exchange plus some admixture of BLYP correlation, is hardly affordable. Hence, the normal procedure is to perform CPMD simulations and to compute the observed reaction intermediates and products in a second step using more accurate approaches. This option, however, is very limited in the case of condensed phase simulations. Most quantum chemical approaches are not implemented with periodic boundary conditions as would be needed for describing a solid or liquid phase. In difficult situations, such as highly reactive systems with many possible reaction pathways, there is no alternative to trusting the results obtained with the Car–Parrinello molecular dynamics code. If we cannot perform further computational checks, Car–Parrinello simulations can merely assist in the intuition of a chemist to explain all of the steps involved in a complex mechanism. CPMD has the advantage that it is possible to test all potential reaction pathways at once. A disadvantage is that chemical reactions are rare events and may not be observed on the picosecond timescale. To overcome this gap, we use very high temperatures.

2. Results and Discussions

In the beginning the performance of the lithium Troullier–Martins pseudopotential and the BLYP functional were checked by varying the size of the unit cell. We found a favorable agreement with a deviation of less than one percent from the experimental value (see the Supplementary Materials, Figure S1).

The simulation protocols are listed in Table 1. We performed simulations for different compositions and temperatures. We started with an equilibration of a pure lithium (100) surface containing four lithium layers. In simulation 1 the stability of the slab was tested. We chose the (100) surface because it is most easily to prepare and to understand and has a similar surface energy as the (111) and (110) surfaces.

In summary, in simulations 3 to 13, the beginning of the formation of lithium nitride species was observed for the system without oxygen. In the simulations 20 and 23, the presence of oxygen enhances the N-H formation, while in simulations 10, 11, and 24 N-H formation occurs without the interaction with oxygen.

In detail: in simulation 1 we find only minor reconstructions (Figures S2 and S3 in the Supplementary Materials). The system relaxes in z direction only. For the distance of the outer two lithium layers the bulk value (1.756 Angstrom) is reduced to 1.660 Angstrom. The distance to the inner layer relaxes even more strongly to 1.378 Angstrom.

While this structure is perfectly stable, we observe a fast reaction if we add nitrogen and hydrogen molecules (Figure 1).

Table 1. Protocol of the CPMD simulations containing nitrogen and hydrogen discussed in this paper. Given are the numbers of Li, N, H, and O atoms in the single models and the initial temperature. Production runs are listed only, not the equilibration runs. Higher temperatures facilitate the reactions, while the effect of pressure is unclear.

System	Simulation Number	Li/N/H/O	Temp. [K]	N-N Cleavage	N-H Formation
Li slab	1	64/0/0/0	300	no	no
Li slab	2	64/24/72/0	300	no	no
Li slab	3	64/20/68/0	300	yes	no
Li slab	4	64/20/64/0	300	yes	no
Li slab	5	64/24/72/0	600	yes	no
Li slab	6	64/20/68/0	600	yes	no
Li slab	7	64/20/64/0	600	yes	no
Li slab	8	64/24/72/0	800	yes	no
Li slab	9	64/20/68/0	800	yes	no
Li slab	10	64/20/64/0	800	yes	yes
Li slab	11	64/24/72/0	1000	yes	yes
Li slab	12	64/20/68/0	1000	yes	no
Li slab	13	64/20/64/0	1000	yes	no
Li slab, O ₂	14	64/20/68/12	300	no	no
Li slab, O ₂	15	64/12/36/8	300	no	no
Li slab, O ₂	16	64/6/18/4	300	no	no
Li slab, O ₂	17	64/20/68/12	600	no	no
Li slab, O ₂	18	64/12/36/8	600	yes	no
Li slab, O ₂	19	64/6/18/4	600	yes	no
Li slab, O ₂	20	64/20/68/12	800	yes	yes
Li slab, O ₂	21	64/12/36/8	800	yes	no
Li slab, O ₂	22	64/6/18/4	800	no	no
Li slab, O ₂	23	64/20/68/12	1000	yes	yes
Li slab, O ₂	24	64/12/36/8	1000	yes	yes
Li slab, O ₂	25	64/6/18/4	1000	yes	no

Hereby, it is the nitrogen molecules that react the most strongly with the surface. In contrast to the behavior of molecules in contact with oxidic surfaces [13–16], we observed that the metallic lithium surface ‘swallows’ the nitrogen molecules within a few picoseconds. In most cases, this leads to an elongation of the nitrogen–nitrogen bond. In most simulations, the complete dissociation of at least one nitrogen molecule was observed. In simulation 2 (see the Supplementary Materials, Figures S4–S6), an undissociated nitrogen molecule is integrated into the lithium bulk, forming a characteristic structure with D_{3h} symmetry (Figure 2). The two nitrogen atoms are surrounded by nine lithium atoms. The three lithium atoms in the middle of the arrangement are coordinated with both nitrogen atoms; hence, each nitrogen atom is coordinated by six lithium atoms. The nitrogen–lithium distances are all in the range of 1.9–2.1 Angstrom, with the distances to the inner nitrogen atoms being a little bit longer, by approximately 0.1 Angstrom on average. The nitrogen–nitrogen bond is elongated to values of approximately 1.7–1.8 Angstrom, but, in this particular simulation, it did not break (Figure 2).

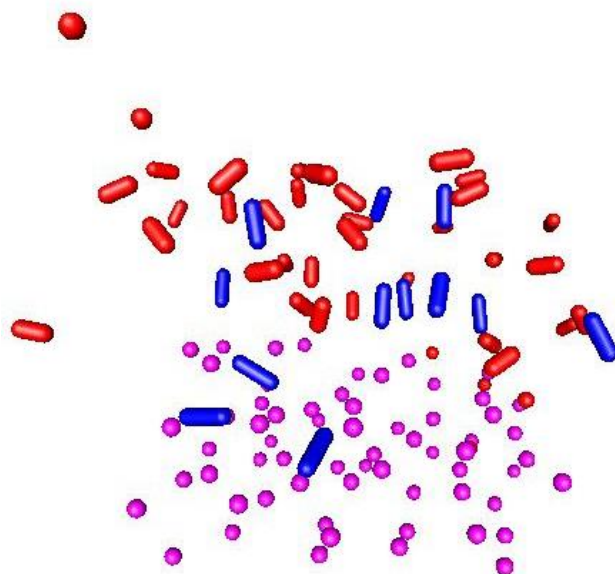


Figure 1. Start of simulation 2 after the equilibration, side view. Blue: nitrogen, red: hydrogen, magenta: lithium.

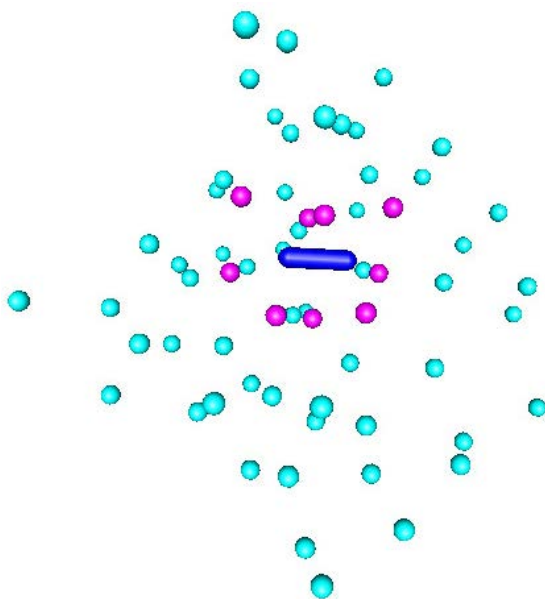


Figure 2. Simulation 2, top view. For a mixture of nitrogen and hydrogen, a fast reaction of nitrogen with the lithium slab was observed. In the figure, only one nitrogen molecule is shown (blue), which is integrated into the bulk. All other nitrogen molecules and the hydrogen molecules are omitted in the graphical representation. The nearest neighbors of the N_2 moiety are highlighted in magenta; all other lithium atoms are turquoise.

It is possible to optimize this Li_9N_2 structure in vacuo and to perform a method comparison for this system (Figure 3 and Table 2). All methods agree well. MP2 shows the largest deviations from the most powerful double-hybrid B2PLYP calculations (Table 2). In particular, the BLYP values are close to that obtained with the much more expensive, but also much more accurate, B2PLYP and CCSD calculations. Dispersion corrections lead to no improvement. The comparison supports the validity of BLYP for the condensed-phase simulations. In contrast to the situation in the bulk, the N-N distance is large enough to be considered as broken. Nevertheless, all methods converge to a perfect D_{3h} structure. Hence, as a consequence of nitrogen interacting with the lithium surface, we obtained a very well-defined structure with strong bonds that is floating in the almost-liquid lithium surrounding.

Table 2. Optimized Li_9N_2 structure, method comparison. Each nitrogen atom is coordinated by six lithium atoms. The inner three lithium atoms are bound to both nitrogen atoms, see Figure 3.

Method	N-N [Å]	Outer Li-N [Å]	Inner Li-N [Å]
BLYP	3.04	1.85	2.02
BLYP/D3BJ	3.02	1.84	2.00
B3LYP	3.03	1.84	2.00
B3LYP/D3BJ	3.01	1.83	1.99
B2PLYP	3.04	1.85	2.01
B2PLYP/D3BJ	3.03	1.85	2.01
MP2	3.11	1.87	2.06
CCSD	3.06	1.86	2.02

This also accounts for structures that result from the breaking of a nitrogen bond. A Li_{11}N_2 structure, as formed in the simulations, can be optimized without the Li surrounding. The result is close to D_{4d} symmetry (Figure 3 and Table 3). While lithium is a ductile metal, these lithium–nitride clusters have a well-defined structure, whereby the deviations from the perfect symmetry are larger for Li_{11}N_2 than for Li_9N_2 ; see Table 3.

Table 3. Optimized Li_{11}N_2 structure, method comparison. Each nitrogen atom is coordinated by six lithium atoms. The two nitrogen atoms share one lithium atom.

Method	N-N [Å]	Outer Li-N [Å]	Central Li-N [Å]	Inner Li-N [Å]
BLYP	3.96	1.85	1.91–1.94	2.00
BLYP/D3BJ	3.89	1.84	1.91–1.93	1.95
B3LYP	3.95	1.84	1.90–1.92	1.98
B3LYP/D3BJ	3.89	1.83	1.90–1.91	1.94
B2PLYP	3.98	1.84	1.92–1.93	1.99
B2PLYP/D3BJ	3.94	1.84	1.92–1.93	1.97
MP2	4.04	1.87	1.94–1.95	2.02
CCSD	4.01	1.85	1.93–1.94	2.01

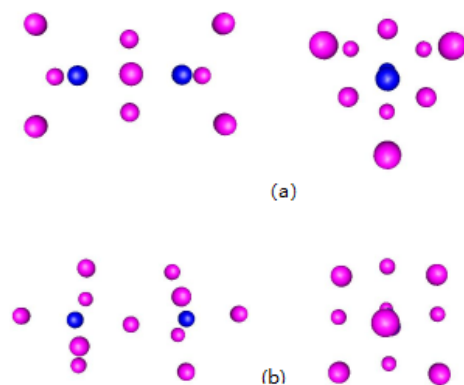


Figure 3. Li_9N_2 (a) and Li_{11}N_2 (b) structures from different perspectives, as observed in the CPMD simulations and then optimized in vacuo (BLYP). Upper row: Li_9N_2 (D_{3h}), lower row: Li_{11}N_2 (D_{4d}). Nitrogen: magenta, lithium: blue. The D_{3h} symmetry of Li_9N_2 and the close-to D_{4d} symmetry of Li_{11}N_2 were not imposed in the input but were obtained from the calculations.

In simulations 3 to 13, we observed at least one nitrogen–nitrogen cleavage after intrusion in the lithium slab. A more detailed analysis of the change of the relevant distances with time is given in the Supplementary Materials for simulations 3 (Figures S7–S11) and 4 (Figures S12–S14). Normally, the nitrogen–nitrogen distance increases rapidly until it reaches a constant value, indicating the integration into the lithium lattice. Only in a few cases is the formation of N-H observed (Figures 4 and 5; see also the Supplementary

Materials). The N-H formation is clearly temperature-dependent and is not observed at low temperatures. Figures 4 and 5 show the mechanism for two nitrogen–nitrogen rupture events in simulation 10. Both reaction sequences start with the N-H bond formation connected with the H-H bond breaking. The N-N bond breaks some picoseconds later. A different sequence is observed in simulation 11 (Figure S15): Here the N-H formation occurs after the breaking of the N-N triple bond. Hence, also this reaction pathway is possible. A further reaction to ammonia was not observed on the time scale of the simulations.

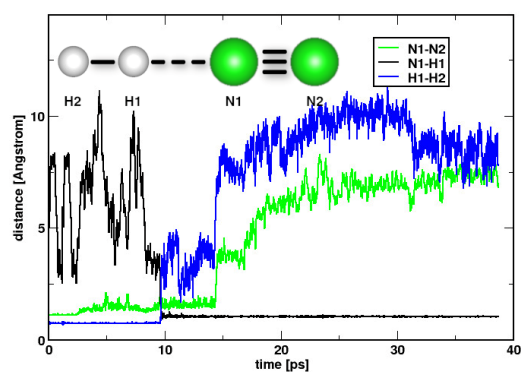


Figure 4. Simulation 10, first reaction: in the beginning, the N-H bond is formed and the H-H bond is broken. The N-N bond breaks a few picoseconds later.

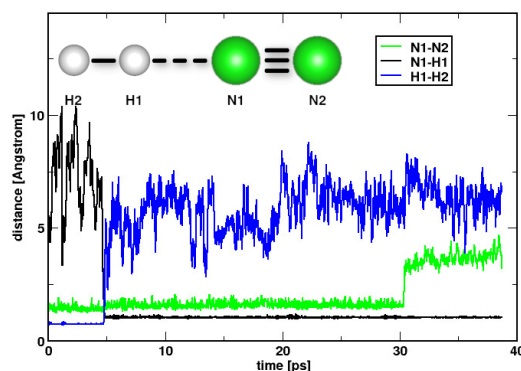


Figure 5. Simulation 10, second reaction: in the beginning, N-H is formed. Almost simultaneously, the H-H bond breaks. A few picoseconds later, the N-N bond is broken.

The next step was to include molecular oxygen in the simulations (Figures 6 and 7, see also the Supplementary Materials, Figures S16 and S17). It turned out that it was hopeless to model the system with oxygen molecules before oxygen adsorption. Oxygen is strongly attracted by the surface and decomposes immediately. It forms surface oxygen ad-atoms and OH groups, thus activating the hydrogen molecules. The oxygen coverage partially inhibits the formation of lithium nitride.

In simulations 20 and 23, oxygen actively participates in the N-H formation. In simulation 23 N-H formation is followed by N-N cleavage (Figure 6). In simulation 20 again the N-N cleavage proceeds N-H formation (Figure S16).

Table 4 lists the coordination numbers of lithium that were obtained during the simulations that led to N-H formation (simulations 10, 11, 20, 23, and 24, with simulations 10 and 23 exhibiting two independent reaction sequences). In the case of simulations 20 and 23, a participation of oxygen in the reaction is observed. Only in a few cases did nitrogen atoms reach the full coordination with six lithium atoms. This is in contrast to what was observed for the clean surface which is not covered by oxygen. Obviously, nitrogen is more easily integrated into the lithium lattice if no surface oxygen inhibits it.

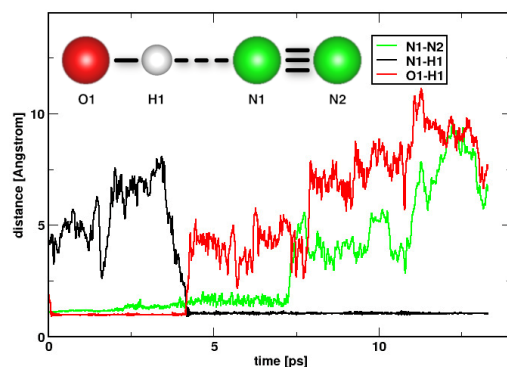


Figure 6. Simulation 23, first reaction: a hydrogen atom is readily transferred from an OH group to nitrogen, causing N-N bond breaking.

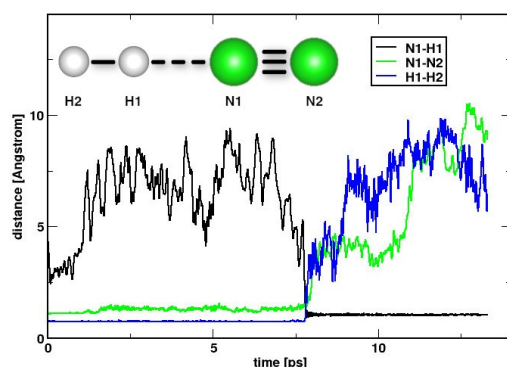


Figure 7. Simulation 23, second reaction: also in the simulations containing oxygen, the oxygen-free reaction can be observed. In the actual case, bond breaking (N-N, H-H) and bond formation (N-H) occur almost simultaneously, with the H-H bond breaking being the fastest.

Table 4. Final coordination numbers of the relevant nitrogen and oxygen atoms with lithium in the simulations where N-H formation was observed. In simulations 10 and 23, two reaction events were monitored. High coordination numbers indicating nitride formation were observed preferably at low temperatures and in the systems without oxygen.

Simulation	Atom	Coordination
10	N	6
10	N	2
10	N	6
10	N	3
11	N	6
11	N	3
20	O	3
20	N	3
20	N	5
23	N	3
23	N	4
23	O	4
23	N	3
23	N	3
24	N	4
24	N	3

3. Conclusions

We observed an ultrafast reaction of molecular nitrogen with the lithium (100) surface. Hydrogen reacts slower with the lithium surface. In contrast to what was found in experiment, we do not necessarily obtain a Li_3N stoichiometry. We find the formation of Li_9N_2

and Li_{11}N_2 clusters. Of course this is just the start of the bulk formation and higher N_2 pressure would easily yield a stoichiometry that is closer to experiment. Hydrogen reacts more slowly with the lithium surface. It has a chance to react with a nitrogen atom in the moment the nitrogen molecule reacts with the surface which leads to N-N cleavage. Once nitrogen is fully integrated into the bulk, it is no longer reactive.

Oxygen is even more reactive than nitrogen. It is difficult at best to equilibrate the surface before oxygen is drawn into the lithium bulk. Oxygen has two effects: firstly, the ultrafast formation of lithium oxide species renders the surface less active and prevents the formation of the corresponding nitride. It can be concluded that this coverage of the catalyst prevents the formation of inactive nitride species that cannot desorb anymore. The second effect of oxygen addition is the generation of active species by attacking the relatively unreactive hydrogen molecules, thus making additional reaction pathways viable. While we can tentatively explain the experimental behavior by this partial poisoning of the catalyst, we were not able to observe the full reaction to ammonia. We can observe, however, two important steps: the breaking of the nitrogen–nitrogen bond and the formation of adsorbed N-H. These two steps can occur simultaneously. It was frequently observed that the lithium surface absorbs one of the nitrogen atoms, whereas the other nitrogen atom reacts with molecular hydrogen. The extremely easy integration of nitrogen and oxygen atoms into the lithium bulk is in line with the extremely low density of the lithium lattice (0.534 g/cm^3 , cf. lithium nitride: 1.294 g/cm^3 , lithium oxide: 2.013 g/cm^3 , beryllium: 1.848 g/cm^3 , boron: 2.460 g/cm^3).

From the above, it is evident that CPMD/BLYP has the accuracy and efficiency to describe heterogeneous catalysis by lithium. Strictly speaking we obtain the high-temperature behaviour, that is, some caution is necessary when interpreting the results. However, also in experiment, high local kinetic energies are to be expected for the exothermic reaction of the lithium surface with nitrogen. Partial melting of the metallic lithium surface may occur, while Li_3N has a higher melting point and forms rigid islands in the metallic surrounding. (Melting point Li: 454 K, Li_3N : 1086 K.) It is also clear, however, that a larger amount of and much longer simulations would yield a more complete picture. Increasing the amount of simulations is not only hindered by the CPU time that is needed, but also by the time that is needed for the evaluation of the complex reaction sequences. Under these circumstances, we can determine and analyze only the most important reaction scenarios.

4. Methods

Ab-initio molecular dynamics simulations [11,12] have been performed with the CPMD code [17] using the Becke–Lee–Yang–Parr (BLYP) functional. The time step was chosen as 5 a.u. (0.1209 fs) and the fictitious electron mass as 400 a.u. Troullier–Martins pseudopotentials as optimized for the BLYP functional were employed for describing the core electrons [18,19]. The plane wave cutoff, which determines the size of the basis set, was set to 50.0 Rydberg. The simulation cell size was chosen as $26.5 \times 26.5 \times 26.5 \text{ a.u.}^3$ ($14.0 \times 14.0 \times 14.0 \text{ Angstrom}^3$) for the periodic systems. This super-cell size corresponds to $4 \times 4 \times 4$ times the size of the bcc unit cell of bulk lithium. After equilibration, the production runs were performed with Nose–Hoover thermostats [20–22] for the electrons and the ions. The Nose parameters were chosen as 0.01 a.u. and $10,000 \text{ cm}^{-1}$ for the electrons and 300 K, 600 K, 800 K, or 1000 K and 3000 cm^{-1} for the ions. Data were accumulated for 37.49 ps (Li slab) and 13.30 ps (Li slab plus oxygen), respectively.

A method comparison for the Li_9N_2 and Li_{11}N_2 clusters in vacuo was performed using the Gaussian program package [23], namely for the density functional methods BLYP [24], BLYP-D3BJ [25,26], B3LYP [27], and B3LYP-D3BJ, in addition for the post-Hartree-Fock methods MP2 and CCSD, and finally for the double hybrid methods B2PLYP [28], and B2PLYP-D3BJ. The latter two methods are a mixture of B3LYP and MP2. The abbreviation D3BJ indicates that the Becke-Johnson damping was used in the D3 dispersion corrections [25,26]. The 6-311G(d,p) basis set was employed.

Supplementary Materials: The following supporting information can be downloaded at: <https://www.mdpi.com/article/10.3390/nitrogen3030026/s1>, Figure S1: Cell constant depending on

the plane wave cutoff for the $3 \times 3 \times 3$ supercell; Figure S2: z-Axis of all the 64 lithium atoms in simulation 1, eight atoms per plot (100 K); Figure S3: z-Axis of all the 64 lithium atoms in simulation 1, eight atoms per plot (300 K); Figure S4: Diatomic distances of all nitrogen molecules in simulation 2 (300 K); Figure S5: Simulation 2: Distances of the nearest neighbors, first nitrogen atom; Figure S6: Simulation 2: Distances of the nearest neighbors, second nitrogen atom; Figure S7: Diatomic distances of all nitrogen molecules in simulation 3 (300 K); Figure S8: Simulation 3: Distances of the nearest neighbors, first nitrogen atom; Figure S9: Simulation 3: Distances of the nearest neighbors, second nitrogen atom; Figure S10: Distances of the nearest neighbors, third nitrogen atom; Figure S11: Distances of the nearest neighbors, fourth nitrogen atom; Figure S12: Diatomic distances of all nitrogen molecules in simulation 4 (300 K); Figure S13: Simulation 4: Distances of the nearest neighbors, first nitrogen atom; Figure S14: Simulation 4: Distances of the nearest neighbors, second nitrogen atom; Figure S15: Simulation 11: Formation of the N-H bond, breaking of the N-N and H-H bonds; Figure S16: Simulation 20: Formation of the N-H bond, breaking of the N-N and O-H bonds; Figure S17: Simulation 24: Formation of the N-H bond, breaking of the N-N and H-H bonds.

Author Contributions: Conceptualization, I.F. and E.N.; methodology I.F.; software, I.F.; validation, I.F., D.M. and D.A.R.; formal analysis, D.M. and D.A.R.; investigation, D.M. and D.A.R.; resources, I.F.; accuracy, D.M. and D.A.R.; writing—original draft preparation, I.F.; writing—review and editing, I.F., E.N., D.M. and D.A.R.; visualization, D.M. and D.A.R.; supervision, I.F.; project administration, I.F.; funding acquisition, I.F. and E.N. All authors have read and agreed to the published version of the manuscript.

Funding: The study was supported by the Deutsche Forschungsgemeinschaft (DFG), grant FR1246/10-1 and by the BMBF, project 01DK20091. Part of the calculations were performed on the local cluster of the Leibniz University of Hannover at the LUIS and on the Höchstleistungsrechner Nord, HLRN, maintained by the North German Supercomputing Alliance, project nic00061.

Data Availability Statement: Input files for CPMD version 4.1 are available on demand from the corresponding author.

Conflicts of Interest: The authors declare no conflict of interest.

Abbreviations

The following abbreviations are used in this manuscript:

AIMD	Ab-Initio Molecular Dynamics
BLYP	Becke-Lee-Yang-Parr density functional
B3LYP	Becke-Lee-Yang-Parr hybrid density functional with three parameters
B2PLYP	Double hybrid functional: B3LYP combined with 2nd order perturbation theory
CCSD	Coupled-Cluster, singles, doubles
CPMD	Car-Parrinello Molecular Dynamics
D3BJ	Dispersion correction 3, Becke-Johnson damping
DFT	Density functional theory
MP2	Moller-Plesset perturbation theory, 2nd order

References

1. Holleman, A.F.; Wiberg, E. *Lehrbuch der Anorganischen Chemie*, 101st ed.; de Gruyter: Berlin, Germany; New York, NY, USA, 1995.
2. Wikipedia. Available online: <https://en.wikipedia.org/wiki/Ammonia%20production> (accessed on 16 June 2022).
3. NIST Chemistry WebBook. Available online: <https://webbook.nist.gov/> (accessed on 16 June 2022).
4. Christensen, C.H.; Johannessen, T.; Sørensen, R.Z.; Nørskov, J.K. Towards an ammonia-mediated hydrogen economy? *Catal. Today* **2006**, *111*, 140. [[CrossRef](#)]
5. Giddey, S.; Badwal, S.P.S.; Kulkarni, A. Review of electrochemical ammonia production technologies and materials. *Int. J. Hydrogen Energy* **2013**, *38*, 14576. [[CrossRef](#)]
6. MacFarlane, D.R.; Choi, J.; Suryanto, B.H.R.; Jalili, R.; Chatti, M.; Azofra, L.M.; Simonov, A.N. Liquefied sunshine: Transforming renewables into fertilizers and energy carriers with electromaterials. *Adv. Mater.* **2020**, *32*, e1904804. [[CrossRef](#)] [[PubMed](#)]
7. Tsuneto, A.; Kudo, A.; Sakata, T. Efficient electrochemical reduction of N_2 to NH_3 catalyzed by lithium. *Chem. Lett.* **1993**, *22*, 851. [[CrossRef](#)]
8. Tsuneto, A.; Kudo, A.; Sakata, T. Lithium-mediated electrochemical reduction of high pressure N_2 to NH_3 . *J. Electroanalytical Chem.* **1994**, *367*, 183. [[CrossRef](#)]

9. Lazouski, N.; Schiffer, Z.J.; Williams, K.; Manthiram, K. Understanding Continuous Lithium-Mediated Electrochemical Nitrogen Reduction. *Joule* **2019**, *3*, 1127. [[CrossRef](#)]
10. Li, K.; Andersen, S.Z.; Statt, M.J.; Saccoccio, M.; Bukas, V.J.; Krempel, K.; Sazinas, R.; Pedersen, J.B.; Shadravan, V.; Zhou, Y.; et al. Enhancement of lithium-mediated ammonia synthesis by addition of oxygen. *Science* **2021**, *374*, 1593. [[CrossRef](#)]
11. Car, R.; Parrinello, M. Unified Approach for Molecular Dynamics and Density-Functional Theory. *Phys. Rev. Lett.* **1985**, *55*, 2471–2474. [[CrossRef](#)]
12. Marx, D.; Hutter, J. *Ab Initio Molecular Dynamics: Basic Theory and Advanced Methods*; Cambridge University Press: Cambridge, UK, 2009.
13. Langel, W.; Parrinello, M. Hydrolysis at stepped MgO surfaces. *Phys. Rev. Lett.* **1994**, *73*, 504. [[CrossRef](#)]
14. Langel, W. Car-Parrinello simulation of H₂O dissociation on rutile. *Surf. Sci.* **2002**, *496*, 141. [[CrossRef](#)]
15. Tachikawa, H. Mechanism of Dissolution of a Lithium Salt in an Electrolytic Solvent in a Lithium Ion Secondary Battery: A Direct Ab Initio Molecular Dynamics (AIMD) Study. *ChemPhysChem* **2014**, *15*, 1604. [[CrossRef](#)] [[PubMed](#)]
16. Carrasco, E.; Brown, M.A.; Sterrer, M.; Freund, H.H.; Kwapien, K.; Sierka, M.; Sauer, J. Thickness-dependent hydroxylation of MgO(001) thin films. *J. Phys. Chem. C* **2010**, *114*, 18207. [[CrossRef](#)]
17. Kirchner, B.; Seitsonen, A.P.; Hutter, J. CPMD, Version 4.1, Copyright IBM Corp 1990–2015. Copyright MPI für Festkörpersforschung Stuttgart 1997–2001. Available online: <http://www.cpmd.org/> (accessed on 25 May 2022).
18. Troullier, N.; Martins, J.L. Efficient Pseudopotentials for Plane-Wave Calculations. *Phys. Rev. B* **1991**, *43*, 1993. [[CrossRef](#)] [[PubMed](#)]
19. Boero, M.; Parrinello, M.; Terakura, K.; Weiss, H. Car-Parrinello study of Ziegler-Natta heterogeneous catalysis: Stability and destabilization problems of the active site models. *Mol. Phys.* **2002**, *100*, 2935–2940. [[CrossRef](#)]
20. Nosé, S. A molecular dynamics method for simulations in the canonical ensemble. *Mol. Phys.* **1984**, *52*, 255. [[CrossRef](#)]
21. Nosé, S. A unified formulation of the constant temperature molecular dynamics methods. *J. Chem. Phys.* **1984**, *81*, 511. [[CrossRef](#)]
22. Hoover, W.G. Canonical dynamics: Equilibrium phase-space distributions. *Phys. Rev. A* **1985**, *31*, 1695. [[CrossRef](#)]
23. Frisch, M.J.; Trucks, G.W.; Schlegel, H.B.; Scuseria, G.E.; Robb, M.A.; Cheeseman, J.R.; Scalmani, G.; Barone, V.; Petersson, G.A.; Nakatsuji, H.; et al. *Gaussian-16 Revision A.03*; Gaussian Inc.: Wallingford, CT, USA, 2016.
24. Becke, A. Density-Functional Exchange-Energy Approximation with Correct Asymptotic Behavior. *Phys. Rev. A* **1988**, *38*, 3098–3100. [[CrossRef](#)]
25. Grimme, S. Semiempirical GGA-type density functional constructed with a long-range dispersion correction. *J. Comput. Chem.* **2006**, *27*, 1787–1799. [[CrossRef](#)]
26. Becke, A.D.; Johnson, E.R. A simple effective potential for exchange. *J. Chem. Phys.* **2006**, *124*, 221101. [[CrossRef](#)]
27. Becke, A. A New Mixing of Hartree-Fock and Local-Density Functional Theories. *J. Chem. Phys.* **1993**, *98*, 1372–1377. [[CrossRef](#)]
28. Grimme, S. Semiempirical hybrid density functional with perturbative second-order correlation. *J. Chem. Phys.* **2006**, *124*, 034108. [[CrossRef](#)] [[PubMed](#)]